Chinese Medical Journal®

Association of copy number variation in X chromosome-linked *PNPLA4* with heterotaxy and congenital heart disease

Han Gao[1,2], Xianghui Huang[3], Weicheng Chen[1], Zhiyu Feng[1,2], Zhengshan Zhao[1,2], Ping Li[1,2], Chaozhong Tan[1,2], Jinxin Wang[1,2], Quannan Zhuang[1,2], Yuan Gao[1,2], Shaojie Min[1,2], Qinyu Yao[1,2], Maoxiang Qian[1], Xiaojing Ma[1,2], Feizhen Wu[1], Weili Yan[1,2,4], Wei Sheng[1,2,3,4], Guoying Huang[1,2,3,4]

[1]Children's Hospital of Fudan University, Shanghai 201102, China;
[2]Shanghai Key Laboratory of Birth Defects, Shanghai 201102, China;
[3]Fujian Key Laboratory of Neonatal Diseases, Xiamen Children's Hospital, Xiamen, Fujian 361006, China;
[4]Research Unit of Early Intervention of Genetically Related Childhood Cardiovascular Diseases, Chinese Academy of Medical Sciences, Shanghai 201102, China.

Abstract

Background: Heterotaxy (HTX) is a thoracoabdominal organ anomaly syndrome and commonly accompanied by congenital heart disease (CHD). The aim of this study was to analyze rare copy number variations (CNVs) in a HTX/CHD cohort and to examine the potential mechanisms contributing to HTX/CHD.

Methods: Chromosome microarray analysis was used to identify rare CNVs in a cohort of 120 unrelated HTX/CHD patients, and available samples from parents were used to confirm the inheritance pattern. Potential candidate genes in CNVs region were prioritized via the DECIPHER database, and *PNPLA4* was identified as the leading candidate gene. To validate, we generated *PNPLA4*-overexpressing human induced pluripotent stem cell lines as well as *pnpla4*-overexpressing zebrafish model, followed by a series of transcriptomic, biochemical and cellular analyses.

Results: Seventeen rare CNVs were identified in 15 of the 120 HTX/CHD patients (12.5%). Xp22.31 duplication was one of the inherited CNVs identified in this HTX/CHD cohort, and *PNPLA4* in the Xp22.31 was a candidate gene associated with HTX/CHD. *PNPLA4* is expressed in the lateral plate mesoderm, which is known to be critical for left/right embryonic patterning as well as cardiomyocyte differentiation, and in the neural crest cell lineage. Through a series of *in vivo* and *in vitro* analyses at the molecular and cellular levels, we revealed that the biological function of *PNPLA4* is importantly involved in the primary cilia formation and function via its regulation of energy metabolism and mitochondria-mediated ATP production.

Conclusions: Our findings demonstrated a significant association between CNVs and HTX/CHD. Our data strongly suggested that an increased genetic dose of *PNPLA4* due to Xp22.31 duplication is a disease-causing risk factor for HTX/CHD.

Keywords: *PNPLA4*; Copy number variations; X-chromosome; Heterotaxy; Congenital heart diseases

Introduction

Heterotaxy (HTX) is a rare thoracoabdominal organ anomaly syndrome associated with a spectrum of cardiac and extracardiac malformations and results from the dysregulation of the patterning of the left–right body axis, largely due to dysfunctional cilia.[1] HTX is a relatively rare congenital malformation with an incidence of 1 in 10,000–20,000 live births,[2] while the prevalence of congenital heart diseases (CHDs) is reported to be 8.98 per 1000 live births.[3] HTX frequently occurs with CHDs,[4] and a combination of HTX and CHDs has been found to cause higher mortality and morbidity than the corresponding isolated CHDs,[5] which has drawn greater attention to the underlying causes of these diseases. The co-occurrence of HTX and CHDs (67.7% of HTX patients exhibit complex CHDs and 9.3% of HTX patients exhibit simple CHDs[4]; while among CHD patients, around 1% have HTX) indicates the importance of elucidating the unique underlying genetic pathways of the left–right patterning disturbance that are directly intertwined with the pathogenesis of congenital heart defects.[6] Extensive research has been conducted to investigate the genetic pathogenesis of HTX and CHDs, resulting in the discovery of a series of genetic variants critically contributing to HTX and associated CHDs, such as variants in *ZIC3*,

Access this article online

Quick Response Code:

Website: www.cmj.org

DOI: 10.1097/CM9.0000000000003192

Han Gao, Xianghui Huang and Weicheng Chen contributed equally to this work.

Correspondence to: Guoying Huang, Pediatric Heart Center, Children's Hospital of Fudan University, Shanghai 201102, China
E-Mail: gyhuang@shmu.edu.cn;
Wei Sheng, Shanghai Key Laboratory of Birth Defects, Children's Hospital of Fudan University, Shanghai 201102, China
E-Mail: sheng_wei@fudan.edu.cn

Chinese Medical Journal 2024;137(15)

Received: 25-10-2023; **Online:** 08-07-2024 **Edited by:** Jing Ni

ACVR2B, LEFTY1, LEFFY2, NODAL, NPHP4, and *DNAH5*.[7–11] Most of these genes are critical for left–right patterning during early embryonic development.[12,13] The asymmetrical morphogenetic signaling in the node known as the left–right organizer includes members of the tumor growth factor (TGF)-β family, Nodal and Lefty, which are activated via leftward nodal flow that is generated by motile cilia.[14] Importantly, non-motile cilia are generally considered antenna-like sensory organelles and play key roles in signal transduction.[15] Under the two-cilia model,[16,17] non-motile primary cilia play an essential role in left–right axis specification by sensing nodal flow. However, the currently known mutated genes account for only 15–26% of all HTX cases.[18]

Genome-wide rare copy number variations (CNVs), such as complex chromosomal rearrangements and submicroscopic duplications and deletions, are known to be significant genetic contributors to various congenital defects,[19,20] including CHDs.[21] CNVs are a major category of human genetic variants that can encompass all or part of the intronic and exonic gene regions. Several previous studies have investigated the occurrence of CNVs in HTX and CHD patients and have clearly revealed that CNVs are candidate disease-causing factors for HTX.[22,23] In the present study, we established an HTX/CHD patient cohort and screened for rare CNVs using a chromosome microarray, followed by *in vivo* and *in vitro* analyses at the cellular and molecular levels to validate our genetic data on the potential biological function of *PNPLA4*. Using this approach, we identified *PNPLA4* within a CNV region on the X chromosome (Xp22.31) as a candidate gene contributing to HTX/CHD via its role in regulating energy metabolism and non-motile cilia formation and function.

Methods

Ethical approval

This study was approved by the Institutional Ethics Committee of Children's Hospital of Fudan University (CHFU) (No. [2021]429). Written informed consent was obtained from the parents/guardians of the participants.

Study population and phenotypic assessment

The participants were recruited from the CHFU and included 120 unrelated HTX patients with CHDs from January 2013 to September 2018 [Supplementary Table 1, http://links.lww.com/CM9/C59]. The median age at diagnosis was 3.16 years (interquartile range: 0.66–5.87 years). In all, 44 patients were females (36.7%), and 76 were males (63.3%). The diagnosis of all patients in the cohort was confirmed by imaging examination[5] and categorized based on the classification described previously.[2,24]

Chromosome microarray analysis (CMA)

Genomic DNA was extracted from blood samples with a QIAamp DNA Blood Midi Kit (Qiagen, Hilden, Germany) in accordance with the manufacturer's protocol. Both the Agilent (Santa Clara, USA) microarray kit (100 patients) and Affymetrix (Santa Clara, CA, USA) microarray kit (20 patients) were used for CMA, depending on the availability at the time of testing. CNV calls were made using the standard protocol of the Chromosome Analysis Suite (Thermo Fisher, Waltham, USA) and Genoglyphix software (PerkinElmer, Waltham, USA). The annotations for the breakpoints refer to the human reference sequence GRCh37 (hg19). Rare CNVs were defined as CNVs (size ≥20 kb) with no more than four occurrences in the Database of Genomic Variants database (http://http://dgv.tcag.ca/) of common CNVs (>50% overlapping).[25] To interpret rare CNVs, we searched the DatabasE of genomiC varIation and Phenotype in Humans using Ensembl Resources database (https://decipher.sanger.ac.uk/) and Online Mendelian Inheritance in Man (http://omim.org) for clinical relevance.

Human induced pluripotent stem cells (hiPSCs) culture and generation of PNPLA4-overexpressing hiPSCs

Wild-type hiPSCs were generated previously.[26] The hiPSCs were plated on Matrigel-coated dishes supplemented with mTeSR-1 stem cell culture medium (STEMCELL Technologies, Vancouver, Canada). Cardiac differentiation procedures were adapted from a previously published article.[27] During differentiation, the cells were incubated with Roswell Park Memorial Institute (RPMI) 1640 medium supplemented with 2% B27 minus insulin (RPMI/B27-I, Gibco, Waltham, USA) for 7 days. On Days 1–2, the cells were supplemented with 7 μmol/L CHIR99021; on Days 4–5, 5 μmol/L IWR-1 was added to the medium. To generate *PNPLA4*-overexpressing and control pLVX-hiPSCs, we infected cells with lentivirus containing the pLVX plasmid and selected positively transfected cells with 2 μg/mL puromycin. These pooled positively transfected cells were maintained and subjected to a cardiomyocyte differentiation protocol in subsequent experiments.

Zebrafish manipulation

Adult zebrafish of the Tg (cmcl2-eGFP) line were raised and bred under suitable aquaculture conditions at 28.5°C. Approval for all zebrafish experiments was obtained from the CHFU in compliance with standard protocols and regulations.

The complementary DNAs (cDNAs) of *pnpla4* (NM_001142389.1) and *mCHERRY* were synthesized and purchased from Generay Biotech Inc. (Shanghai, China). The complementary DNA (cDNA) fragments were inserted into the pCS2 + vector and transcribed *in vitro* into full-length mRNA with an mMessage mMachine Kit (Invitrogen, Waltham, USA). To ensure global overexpression of mRNA, 100 pg of mRNA was injected during the one-cell stage. To achieve Kupffer's vesicle (KV)-specific overexpression, we adopted a methodology previously described by Zhang *et al*[28] in which mRNAs (100 pg) were injected into the yolk at the 512-cell stage (2.75–3.00 hours post fertilization, hpf) since only progenitor cells of dorsal forerunner cells in KV retain a cytoplasmic

bridge with yolk cells.[29] Embryos were imaged using Leica M205C and Leica SP8 confocal microscopes (Leica, Wetzlar, Germany).

AC16 culture and generation of PNPLA4-overexpressing AC16 cells

The AC16 cell line was previously derived from human cardiomyocytes.[30] We obtained the AC16 cell line from the Cell Bank, Shanghai Institute of Biochemistry and Cell Biology (serial number: SCSP-555, Shanghai, China). All cells were cultured in Dulbecco's Modified Eagle Medium (DMEM) supplemented with 4.5 g/L glucose and 10% fetal bovine serum (FBS) (Corning, New York, USA) at 37°C and 5% CO_2. To generate *PNPLA4*-overexpressing AC16 cells, cDNA from the human *PNPLA4* gene (NM_004650.3) was subcloned and inserted into a pcDNA3.1 vector with a tailed Flag tag. Lipofectamine 3000 (Invitrogen) was used to transfect pcDNA3.1_*PNPLA4* and control pcDNA3.1 in accordance with the manufacturer's instructions. To achieve inhibition of respiration, 0.2 μmol/L rotenone (dissolved in 0.1% dimethyl sulfoxide [DMSO]; Sigma-Aldrich, USA) was added after 6 h of transfection; 0.1% dimethylsulfoxide was used as the negative control. After 24 h of culture, the AC16 cells were harvested for subsequent experiments.

Western blotting

Total protein extraction was conducted with the addition of prechilled radio immuno precipitation assay (RIPA) buffer (Thermo Fisher Scientific) containing the Halt protease/phosphatase inhibitor cocktail (Thermo Fisher Scientific). Nuclear and cytoplasmic fractions were collected via a nuclear and cytoplasmic protein extraction kit (Beyotime, Shanghai, China). Protein concentrations were measured with a Biochanin-A (BCA) protein assay kit (Takara, Kusatsu, Japan) in accordance with the manufacturer's protocol. The primary antibodies used in this study were as follows: anti-ADP-ribosylation factor-like protein 2 (ARL2) antibody from Abcam, Cambridge, UK (Cat# ab183510; 1:1000 dilution); anti-VDAC antibody from Cell Signaling Technology, Danvers, USA (Cat# 4866S; 1:1000 dilution); anti-β-actin antibody from Proteintech, Wuhan, China (Cat# 81115; 1:5000 dilution); and anti-rabbit horseradish peroxidase (HRP) antibody from Abcam (Cat# ab205718; 1:5000 dilution). The densities of the protein bands were measured with Image Lab software (Version 6.0.1, Bio-Rad, Hercules, USA).

Metabolomic analysis

Metabolomic profiling via ultra-performance liquid chromatography–mass spectrometry (LC–MS) was performed on a Vanquish Ultra High Performance Liquid Chromatography System (Thermo Fisher) by Panomix Inc. (Suzhou, China). The metabolites were measured at a semiquantitative level and further analyzed via Metabolomics Pathway Analysis (MetPA, Metabolomics Innovation Centre, Edmonton, Canada) pathway annotation.[31] To confirm the adenosine triphosphate (ATP) intracellular content, we used a Beyotime ATP Assay Kit (Cat# S0026B, Beyotime) following the manufacturer's protocol. In brief, AC16 cells and 10 embryos at 36 hpf were lysed with prechilled lysis buffer. The lysates were centrifuged at 12,000 × *g* for 5 min. The supernatant was collected, and 20 μL of sample was added to a 96-well view plate with 100 μL of substrate mixture for a luminescence assay (Thermo Fisher). A standard curve was generated in the range of 0.01–10.00 μmol/L, and the ATP content was normalized to the total protein concentration using a bicinchoninic acid protein assay kit (Takara).

Genome-wide transcriptomic analysis

Total RNA was extracted using TRIzol reagent (Invitrogen) in accordance with the manufacturer's protocol. Reverse transcription and sequencing were performed at Novogene, Inc. (Shanghai, China). The raw paired-end read data were obtained and processed with a standard pipeline for data cleaning. The data were aligned with the reference human genome (hg38). Differentially expressed genes (DEGs) were analyzed with the Cufflinks package, with a *P* value of 0.05 indicating significance. Further functional annotation and pathway analysis were conducted via the clusterProfiler (R package available in Bioconductor platform). Clustering analysis were conducted via Mfuzz (R package available in Bioconductor platform).

Single-cell transcriptomic analysis

We analyzed the single-cell RNA sequencing (scRNA-seq) data of human embryos at 4–6 weeks of age from a previously published dataset deposited in the GEO database (GSE157329).[32] We extracted three cell subgroups associated with the viscera, namely, "limb-viscera", "viscera", and "viscera-lowerTrunk". The data were processed using the R package Seurat 4.1.1 (available in https://satijalab.org/seurat/), as described in the previous report.[32] Following normalization, the data were reanalyzed with dimensionality reduction using principal component analysis (PCA) and uniform manifold approximation and projection (UMAP). The annotation of each cluster was based on the original report.[32] The expression profiles of members of the *PNPLA* family across these clusters were determined using the VlnPlot function [Supplementary Figure 7, http://links.lww.com/CM9/C59].

Immunofluorescence staining

AC16 cells were cultured in 20 mm-diameter glass-bottom cell culture dishes (Nest Scientific, Woodbridge, USA). For cilia staining, cells on glass-bottom dishes were cultured in 0.1% FBS DMEM for 2 days before fixation to obtain G0-synchronized cells. After fixation with 4% paraformaldehyde for 20 min at room temperature and permeabilization with 0.5% PBST (Triton X-100/PBS), the cells were blocked in 5% bovine serum albumin and incubated overnight with primary antibodies at 4°C. The primary antibodies used were as follows: DYKDDDDK tag (Cat# 66008, 1:1000; Proteintech, Wuhan, China) and acetylated alpha tubulin (Cat# ab179484, 1:1,000; Abcam). Nuclear staining was performed with 25 mg/mL

4′,6-diamidino-2-phenylindole (DAPI) (Sigma-Aldrich), and 0.33 μmol/L Alexa Fluor 555 Phalloidin (Cell Signaling Technology, Danvers, USA) was used for F-actin staining. The cilia length was measured using ImageJ 2.1.0 (National Institutes of Health, Bethesda, USA)

Statistical analysis

GraphPad Prism (version 7.0, GraphPad Software Inc., La Jolla, USA) was used to analyze the data. Student's *t*-test was employed for the statistical analyses, and a significant *P* value was defined as <0.05.

Results

Identification of rare CNVs and candidate genes in patients

A total of 120 DNA samples from unrelated individuals who had been clinically diagnosed with HTX/CHD were included in this study. The detailed clinical features of all patients are summarized in Supplementary Table 1, http://links.lww.com/CM9/C59. We performed CMA analysis to identify potential novel rare CNVs that were associated with our HTX/CHD cohort.

We identified 17 rare CNVs [Supplementary Table 2, http://links.lww.com/CM9/C59] in 15 of the 120 patients (12.5%) according to the filtering criteria (i.e., size ≥20 kb and no more than four occurrences of >50% overlap in the Database of Genomic Variants dataset). The clinical characteristics of patients harboring rare CNVs are summarized in Supplementary Tables 3, 4, http://links.lww.com/CM9/C59, indicating that the most frequent CHD in CNV-positive CHD/HTX patients was TGA. These CNVs included 15 genic and 2 non-genic CNVs. The 15 genic CNVs included 7 duplication CNVs and 8 deletion CNVs. A schematic overview of the chromosomal locations of all 15 genic CNVs is shown in Figure 1A. Seven of these rare CNVs were reported to be associated with complex syndromes, including cardiac phenotypes [Supplementary Table 2, http://links.lww.com/CM9/C59]. Among all the patients with these 15 rare genic CNVs, parental DNA samples were only available from five patient families for further testing of inheritance patterns. Our analyses revealed that three CNVs (16p12.2 deletion, 2p16.3 duplication, and 14q13.1 duplication) were inherited from unaffected parents. One CNV (15q13.3 deletion) was confirmed to be *de novo*, and one X chromosome CNV (Xp22.31 duplication) in a male proband was inherited from his asymptomatic heterozygous mother, a potential X-linked inheritance. Hence, this Xp22.31 duplication was further investigated. This patient exhibited cardiac malposition (mesocardia, as shown in Figure 1B), and ventricular situs inversus), as well as congenital heart defects, including TGA, VSD, PA, and atrial septal defect. This duplication of Xp22.31 (6456777–8119328) is shown in Figure 1B.

The *PUDP*, *STS*, *PNPLA4*, and *VCX* genes are located within the Xp22.31 region. The *PUDP* gene encodes a pseudouridine 5′-phosphatase and has thus far not been associated with any particular genetic disease.[33] The *STS* gene encodes steroid sulfatase, an enzyme involved in steroid regulation, and was reported to be associated with X-linked ichthyosis.[34] The *VCX* gene belongs to the sex chromosome gene family and is exclusively expressed in sperm.[35] *PNPLA4* is a member of the patatin-like family of phospholipases and functions in lipid metabolism and retinol metabolism.[36] We used the DECIPHER database to assess the correlation between these four genes inside Xp22.31 and cardiac malformation in the patients who harbored CNVs covering these genes (size less than 5 MB). The 18 patients with CNVs (13 duplications and 5 deletions) covering the *PNPLA4* gene exhibited cardiac defects, implying a great possibility of genetic association of *PNPLA4* to HTX and/or CHDs in our cohort [Figure 1C]. Moreover, a loss-of-function variant in the *PNPLA4* gene has been reported to be linked to mitochondrial respiratory chain complex deficiencies.[37]

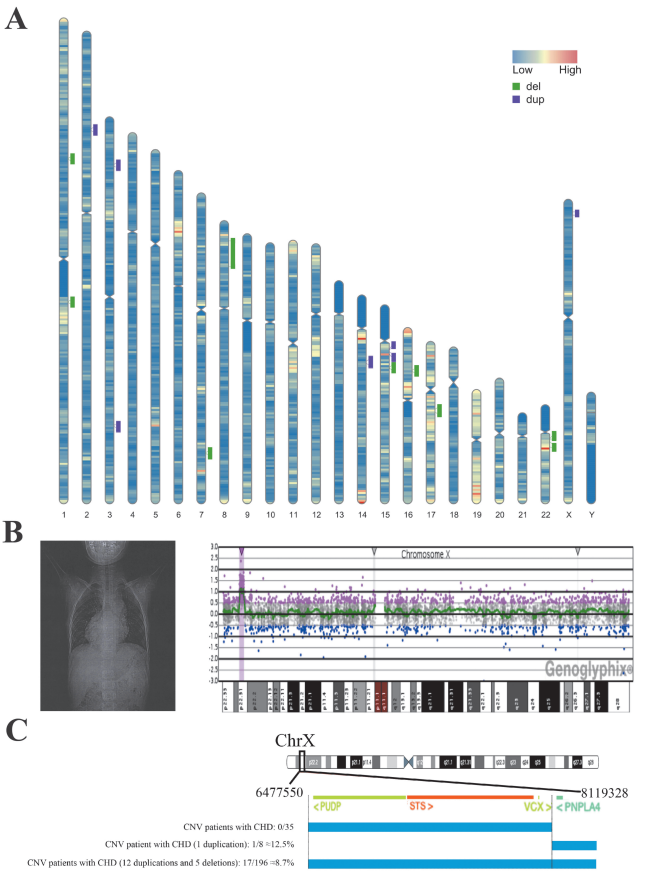

Figure 1: CNVs are associated with HTX/CHD. (A) Regions of copy number gain (purple) and copy number loss (green) are marked in the schematic overview of different chromosomes; the density of gene distribution is as indicated; (B) X-ray image of the patient (left panel) and a magnified view of the chromosomal gain within the Xp22.31 region (right panel); (C) Summary of the clinical features of patients in the DECIPHER database within the Xp22.31 region revealed that only patients with CNVs covering *PNPLA4* exhibited the CHD phenotype. CHD: Congenital heart disease; CNVs: Copy number variations; HTX: Heterotaxy.

Expression pattern of PNPLA4 during the differentiation of hiPSCs into cardiomyocytes

PNPLA4 encodes a member of the patatin-like family of phospholipases.[38] Previously, PNPLA4 was shown

to have both triacylglycerol lipase and transacylase activities and may be involved in adipocyte triglyceride homeostasis in human cells.[39,40] Interestingly, according to genomic databases and published data, mice do not have *PNPLA4* homologs.[36] To understand the role of *PNPLA4* in early development and cardiogenesis, we first analyzed the expression pattern of *PNPLA4* in hiPSC-cardiomyocyte differentiation. Based on our RNA-seq data generated from samples collected from Day 0 to Day 9 of normal hiPSC-cardiomyocyte differentiation, we detected a unique pattern of *PNPLA4* expression. In our hiPSC differentiation system,[27] Day 0 represents the undifferentiated stage, Days 2/3 correspond to the mesodermal differentiation stage, Days 4/5 represent the cardiogenic mesodermal stage, Days 6/7 represent the cardiac progenitor stage, and Days 8/9 represent the early cardiomyocyte stage.[30] Unique gene expression patterns at the whole-genome scale were clustered into 15 categories by using Mfuzz software [Supplementary Figure 1, http://links.lww.com/CM9/C59].[41] Among these clusters, genes known to be associated with HTX were enriched in Clusters 4, 6, and 8 [Figure 2A]. Notably, *ZIC3*[7] was part of Cluster 8, and *Nodal*[12] and *ARMC4*[42] were part of Cluster 6 [Figure 2A]. In both Clusters 8 and 6, their major early expression peak at Day 2 of differentiation is consistent with these genes playing a critical role in the early differentiation stage, e.g., left–right patterning. Interestingly, *ACVR2B*,[43] *PITX2*,[44] and *PNPLA4* were categorized in Cluster 4 [Figure 2A], which exhibited typical activation on Day 2 and peak expression at Days 6/7, suggesting that *PNPLA4* contributes to two different biological functions in the early embryonic patterning and cardioprogenitor/cardiomyocyte differentiation stages. A total of 61 cilia-related genes[45] (out of 160 genes) matched the expression patterns of Clusters 4, 6, and 8, with the majority in Cluster 6, as shown in Supplementary Table 5, http://links.lww.com/CM9/C59.[45] The expression of the cardiac transcription factor NKX2.5, categorized into Cluster 2, initiated at the cardiogenic progenitor stage on Days 4/5 [Figure 2A].

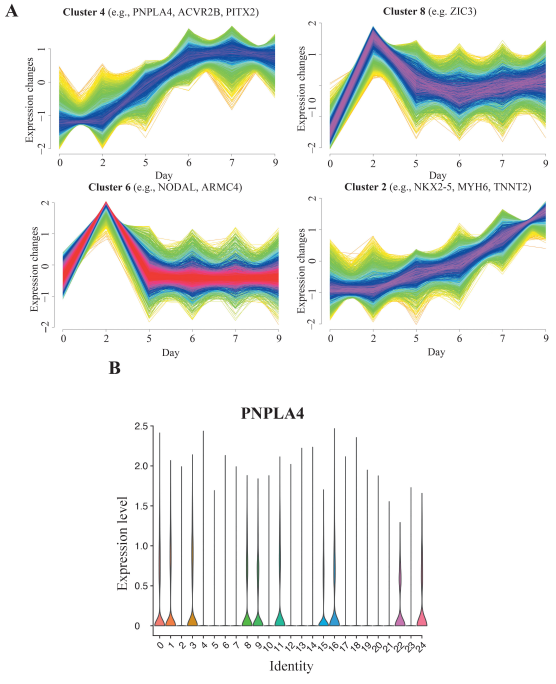

Figure 2: Expression clustering analysis of iPSC-cardiomyocyte differentiation. (A) The time course expression patterns of genes during the differentiation of iPSCs into cardiomyocytes were analyzed by Mfuzz R package. Red and purple indicate high MEM.SHIP values, and yellow and green indicate low MEM.SHIP values. Genes in Cluster 4, including *ACVR2B*, *PITX2*, and *PNPLA4*, exhibited a minor peak on Day 2 and a major peak on Days 6/7. Genes in Clusters 6 and 8, including *ZIC3*, *ARMC4*, and *NODAL*, showed peak on Day 2. Genes in Cluster 2, including *NKX2-5*, *MYH6*, and *TNNT2*, showed different expression patterns; (B) Violin plots of *PNPLA4* gene expression patterns across cellular clusters in human early embryos. Clusters 3, 11, and 16 belong to the lateral plate mesoderm, and Cluster 9 belongs to the neural crest cells. MEM: Membership.

To confirm *PNPLA4* expression in early human embryos, we analyzed the distribution of cells expressing *PNPLA4* in the early organogenesis stage (weeks 4–6) of human embryos using previously published and deposited scRNA-seq sequencing data.[32] The data were acquired from the GEO database (GSE157329). The annotation of the clusters was generated based on the annotation of the developmental system according to the original article.[32] As shown in Figure 2B, *PNPLA4* expression was enriched in clusters from the lateral plate mesodermal lineage (Clusters 3, 11, and 16), which is known to be involved in left–right patterning as well as the differentiation of cardiomyocytes. In addition, *PNPLA4* was also expressed in neural crest lineages (Cluster 9), including cardiac neural crest cells, which are known to be closely associated with cardiogenesis and congenital heart defects.

Collectively with these analyses, we envisioned that the increased genetic dose of *PNPLA4* may have a significant impact on early mesodermal differentiation and/or mesodermal cellular function at the critical earlier time point for left–right asymmetric determination as well as cardiac development or function at a later stage.

Overexpression of PNPLA4 in hiPSCs alters early developmental patterning

To validate the biological impact of the increased *PNPLA4* expression, we generated *PNPLA4*-overexpressing hiPSCs via the use of a lentivirus-based gene expression system (pLVX). There was about 2.4-fold increase of *PNPLA4* mRNA levels in the *PNPLA4*-overexpressing hiPSCs when compared to control hiPSCs [Figure 3A] (0.0009 ± 0.0003 *vs.* 0.0025 ± 0.0002, $t = 7.626$, $P = 0.0016$). *PNPLA4*-overexpressing and control hiPSCs were then subjected to the cardiomyocyte differentiation protocol,[27] followed by transcriptomic analyses on Days 0, 2, and 5 of differentiation [Figures 3B–D]. There was no obvious change in gene expression in *PNPLA4*-overexpressing hiPSCs on Day 0 [Figure 3B], while approximately 567 DEGs were detected on Day 2 [Figure 3C], and 225 DEGs were detected on Day 5 [Figure 3D]. Gene Ontology (GO) term enrichment analysis of the 279 downregulated genes in *PNPLA4*-overexpressing hiPSCs on Day 2 revealed that the top altered Biological Process (BP) enrichments were involved in the embryonic early patterning and specification, which included pattern specification and heart development [Figure 3E]. A representative heatmap of DEGs is shown in Supplementary Figure 2, http://links.lww.com/CM9/C59.

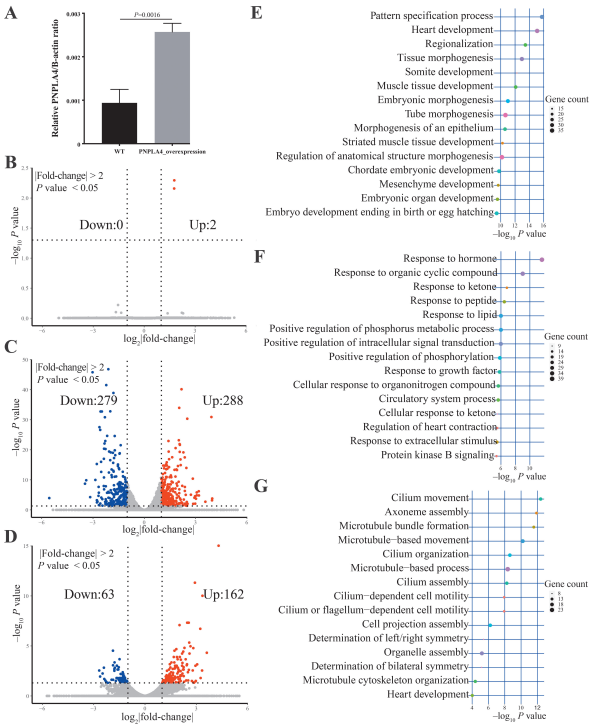

Figure 3: Functional enrichment of transcriptomic data of *PNPLA4*-overexpressing hiPSCs during cardiomyocyte differentiation. (A) qRT–PCR validation of *PNPLA4* expression in the control group and overexpression group on Day 0; (B–D) Volcano plots of Days 0, 2, and 5; (E, F) GO–BP enrichment analysis of downregulated (E) and upregulated (F) genes on Day 2. The result refined the pattern specification process and heart development in downregulated genes (E), while it indicated response to lipid, ketone, and positive regulation of phosphate metabolic process in upregulated genes (F); (G) GO–BP enrichment analysis of upregulated genes on Day 5. The analysis indicated enrichment of the upregulated genes in cilium movement and cilium assembly. BP: Biological process; GO: Gene ontology; hiPSCs: human induced pluripotent stem cells.

Notably, *ZIC3*, *LEF1*, *ARMC4*, and *NOG*, which are well-known genes involved in regulating left–right patterning during early embryonic development,[7,46,47] were significantly downregulated, suggesting an impact on left–right patterning. This observation is consistent with our clinical findings and strongly indicates that an increased genetic dose of *PNPLA4* is likely an important genetic risk factor for HTX. Interestingly, the top altered GO–BP enrichments of upregulated genes on Day 2 were relevant to pathways involved in energy metabolism, including the response to hormones, response to organic cyclic compounds, and response to ketones and lipids [Figure 3F], which is consistent with the well-known functions of the triacylglycerol lipase and transacylase activities of *PNPLA4*.[39,40] Representative upregulated genes are highlighted in Supplementary Figure 2, http://links.lww.com/CM9/C59. *PRKAA2*, *FGF21*, *PPARGC1B*, and *CYP1B1* are genes known to be involved in energy metabolism and were upregulated in *PNPLA4*-overexpressing cells on Day 2.[48–51] More importantly, the top enriched GO–BP terms of the 162 genes upregulated on Day 5 were involved in cilium movement and microtube bundle assembly and movement [Figure 3G]. Supplementary Figure 3, http://links.lww.com/CM9/C59 shows a representative heatmap of DEGs on Day 5. This finding suggested the presence of dysfunctional cilia in *PNPLA4*-overexpressing cells on Day 5. Taken together, our genome-wide transcriptomic analyses revealed a potential pathogenetic pathway by which an increased genetic dose of *PNPLA4* leads to molecular disturbances in left–right asymmetric patterning and altered energy metabolism and cilial dysfunction.

Overexpression of pnpla4 in zebrafish disturbs cardiac looping and cardiac function

Largely due to the lack of the mouse homolog of *PNPLA4*, we opted to use zebrafish as the *in vivo* model system to further validate the relevance of *PNPLA4* to the clinical findings. We generated *pnpla4*-overexpression zebrafish by microinjecting *pnpla4* mRNA (100 pg) at the one-cell stage and microinjecting control zebrafish with mCheery mRNA (100 pg). As shown in Figure 4A, *pnpla4* overexpression resulted in a significantly increased percentage of abnormal hearts with L-loops or no loops and a decreased percentage of normal D-loops compared to those in the control group (27/173 [15.6%] *vs.* 91/190 [47.9%], χ^2 = 43.03, P <0.0001). In addition to the left–right patterning defect, pericardiac edema was noted in 31% (65/209) of the *pnpla4*-overexpressing fish, regardless of with or without left–right patterning defect [Figure 4B, right panel, black arrow indicates]. These data suggest that the overexpression of *pnpla4* in zebrafish produces cardiac looping defects and cardiac functional defects.

KV is known to be critical for regulating left–right patterning in zebrafish.[29,52] To further confirm the abnormal looping phenotype in a cell-specific manner, we generated KV-specific *pnpla4*-overexpressing zebrafish by microinjecting mRNA into the yolk at the 512-cell stage (2.75–3.00 hpf), which is based on a method published previously,[29] in which the injected mRNA enters the progenitor cells of dorsal forerunner cells, contributing to KV through the remaining bridges at this stage. KV overexpression of *pnpla4* resulted in a significant increase in abnormal left–right heart looping compared to that in KV-mCherry control fish [Figure 4C] (12/138 [8.7%]

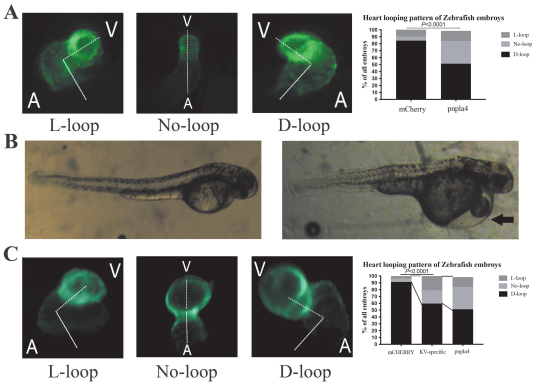

Figure 4: Altered left–right asymmetry and cardiac function in *pnpla4*-overexpressing zebrafish. (A) The abnormal heart looping pattern (L-loop and straight) increased after *pnpla4* overexpression. The left panels show the representative phenotype of *pnpla4*-overexpressing zebrafishes, while the right panel presents the percentage of heart looping phenotypes (n >130); (B) Representative image of pericardial edema (right panel, black marrow) in *pnpla4*-overexpressing zebrafish and normal controls (left panel) of mCHERRY-expressing zebrafishes; (C) KV-specific overexpression of *PNPLA4* replicated part of the abnormal heart looping pattern. The left panels show typical images of heart looping in KV-specific *pnpla4*-overexpressing embryos, while the right panel shows the percentages of heart looping phenotypes (n >130). KV: Kupffer's vesicle.

vs. 118/191 [38.2%], $\chi^2 = 36.45$, $P < 0.0001$). However, no pericardial edema was observed in KV-specific *pnpla4*-overexpressing fish, suggesting that there was no significant alteration in cardiac function. Collectively, these data strongly suggest that the increased expression level of *pnpla4* in KV contributes to the pathogenesis of HTX but is likely not responsible for the potential defect in cardiac function shown in *pnpla4*-overexpressing zebrafish.

PNPLA4 overexpression elevates intracellular ATP production

Previously, PNPLA4 was identified as a phospholipase that is involved in triglyceride and retinylester hydrolysis and likely participates in mitochondrial function and energy metabolism.[37,39] Our transcriptomic data [Figure 3] also demonstrated that multiple metabolic pathways, including multiple pathways related to enhanced energy production, were altered in *PNPLA4*-overexpressing hiPSCs [Figure 3F and Supplementary Figure 2, http://links.lww.com/CM9/C59]. To further analyze these metabolic alterations and their potential link to the pathogenesis of HTX and/or CHDs, we performed untargeted metabolomics in *PNPLA4*-overexpressing cells using an immortalized human cardiomyocyte cell line, AC16. AC16 was previously used to study metabolism and oxidative stress,[53] and a scaled-up culture system was adequate for ultra-performance LC–MS-based metabolomic analysis. We generated transient *PNPLA4*-overexpressing AC16 cells. As shown in Supplementary Figure 4, http://links.lww.com/CM9/C59, Western blotting analysis confirmed the successful generation of *PNPLA4*-overexpressing AC16 cells. Control AC16 cells were transfected with pcDNA3.1. The collected cell lysates were subjected to LC–MS to identify and compare metabolite profiles between *PNPLA4*-overexpressing and control AC16 cells. As shown in Figure 5A, a total of 61 metabolites were differentially expressed between *PNPLA4*-overexpressing AC16 cells and control AC16 cells. Among these altered metabolites, ATP levels [Figure 5A] and the ATP/AMP ratio [Figure 5A] (0.010 ± 0.008 *vs*. 0.012 ± 0.033, $t = 3.154$, $P = 0.0197$) were significantly elevated in *PNPLA4*-overexpressing AC16 cells, which is consistent

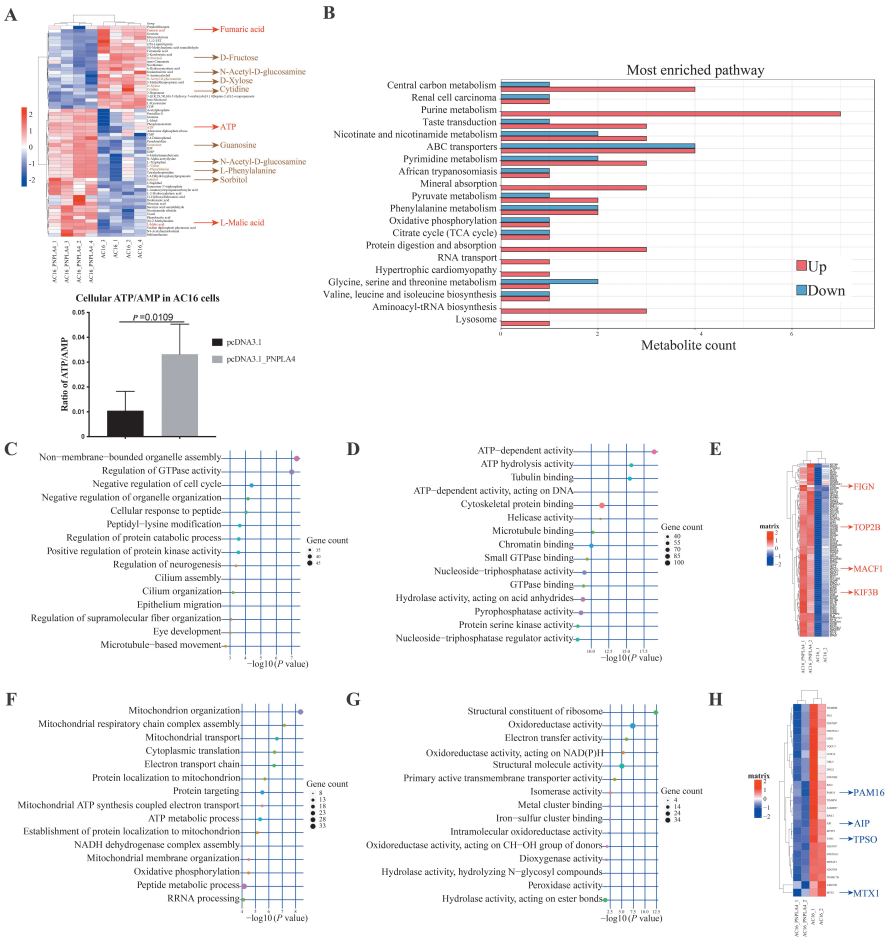

Figure 5: Enhanced energy metabolism in *PNPLA4*-overexpressing AC16 cells. (A) Differentially expressed molecules in untargeted metabolomics between the pcDNA3.1 and pcDNA3.1_*PNPLA4* groups in AC16 cells. In the heatmap of differentially expressed molecules, genes related to ATP-binding cassette (ABC) transporters are shown in brown, while genes related to oxidative phosphorylation and the TCA cycle are shown in red. The bottom panel shows ATP/AMP ratio in *PNPLA4*-overexpressing and control cells; (B) Enrichment analysis of the top-ranked differentially expressed molecules in untargeted metabolomics between the pcDNA3.1 and pcDNA3.1_*PNPLA4* groups in AC16 cells, including purine metabolism, ABC transporters, oxidative phosphorylation, and the TCA cycle; (C–H) Functional enrichment of RNA-seq results between the AC16 and AC16_*PNPLA4* groups; (C) Enrichment of upregulated genes indicated regulation of GTPase activity, microtubule-based movement, and cilium assembly in terms of BP; (D) Enrichment of upregulated genes refined ATP-dependent activity in terms of MF; (E) Representative heatmap of upregulated ATPase-dependent activity; Enrichment of downregulated genes refined ATP synthesis and NADH dehydrogenase activity in terms of BP (F) and MF (G); (H) Representative heatmap of downregulated mitochondrial respiratory chain complex assembly. ATP: Adenosine triphosphate; BP: Biological process; MF: Molecular function.

with the enhanced energy metabolism pathways found in *PNPLA4*-overexpressing hiPSCs. According to the metabolite counts of the top enriched MetPA pathways, these altered metabolites were strongly enriched in the purine metabolism/purinergic signaling pathway, which is a critical pathway controlling intracellular energy homeostasis and nucleotide synthesis [Figure 5B].[54] To further confirm these findings, we measured ATP production in *PNPLA4*-overexpressing AC16 cells and *pnpla4*-overexpressing zebrafish embryos. As shown in Supplementary Figure 5, http://links.lww.com/CM9/C59, cellular ATP levels were significantly elevated in both *PNPLA4*-overexpressing AC16 cells and *pnpla4*-overexpressing zebrafish embryos compared to the respective controls, further supporting our metabolomic analysis.

Genome-wide transcriptomic profiling comparing *PNPLA4*-overexpressing and control AC16 cells was performed. As shown in Supplementary Figure 6, http://links.lww.com/CM9/C59, more than 1600 DEGs were identified between *PNPLA4*-overexpressing and control AC16 cells; 1169 genes were upregulated, while 520 genes were downregulated. Consistent with our findings in *PNPLA4*-overexpressing hiPSCs [Figure 3G], the GO–BP term enrichment analysis of the upregulated genes revealed altered supramolecular fiber organization and cilium assembly in *PNPLA4*-overexpressing AC16 cells [Figure 5C]. As expected, GO-molecular function (MF) enrichment analysis of the upregulated genes revealed upregulated ATPase activity and tubulin binding as the two most altered MFs [Figure 5D], which was consistent with the changes in metabolites [Figure 5A,B]. A representative heatmap is shown in Figure 5E. Notably, the expression of *FIGN*, *MACF1*, *TOP2B*, and *KIF5B* was significantly upregulated in *PNPLA4*-overexpressing AC16 cells [Figure 5E, arrows]. These genes are known to be critically involved in ATPase activity and cardiac development.[55–59] Consistently, multiple ATP-dependent BPs, such as cellular migration and microtubule-based movement [Figure 5D], were among the altered cellular functions. Interestingly, the expression of several genes involved in ATP production and nicotinamide adenine dinucleotide (NADH) dehydrogenase activity was attenuated in *PNPLA4*-overexpressing AC16 cells, likely due to the negative feedback response to increased ATP levels in the cells [Figure 5F,G], which was attributed to the transcriptional downregulation of mitochondrial respiratory chain complex assembly genes [Figure 5H].

Impact of PNPLA4 overexpression on primary cilia formation

As demonstrated above, cilia and microtubule formation or function were also potentially affected in both *PNPLA4*-overexpressing hiPSCs and *PNPLA4*-overexpressing AC16 cells. Previous studies have shown that actin polymerization and motor activity are ATP-dependent and can influence cilium assembly through actin–microtubule crosstalk.[60] Thus, we examined the distribution pattern of filamentous actin (F-actin) in *PNPLA4*-overexpressing AC16 cells. By using phalloidin staining, we detected elevated intracellular accumulation of F-actin patches in *PNPLA4*-overexpressing AC16 cells largely adjacent to the nucleus [Figure 6A, red arrows], suggesting an abnormally enhanced level of actin polymerization, which is consistent with the increase in ATP production and confirms the RNA-seq results.[61,62] As elevated F-actin polymerization is known to affect the transport of cargo to primary cilia, such as GTPases and intraflagellar transport complex proteins,[63,64] we postulated that the primary cilia formation was affected in *PNPLA4*-overexpressing AC16 cells. As shown in Figure 5C,D, GTPase activity and its related pathway were enriched in *PNPLA4*-overexpressing AC16 cells, supporting our findings. Among GTPases, ARL2 has well-defined functions in both primary cilia and mitochondria. ARL2 has been reported to process primary cilia assembly in the cytoplasm and regulate oxidative metabolism in mitochondria.[65,66] Western blotting analysis was used to determine the total cellular level of ARL2, and we found that ARL2 was significantly downregulated in *PNPLA4*-overexpressing AC16 cells [Figure 6B] (relative expression to control group, 0.748 ± 0.139, $t = 3.138$, $P = 0.0349$). Furthermore, we confirmed that cytoplasmic ARL2, but not mitochondrial ARL2, was downregulated [Figure 6B] (relative expression to control group, 0.806 ± 0.087, $t = 3.861$, $P = 0.0181$), suggesting that primary cilia formation is impaired.

Primary cilia are immotile cilia that have been reported to be affected by ATP imbalance and are relevant to the pathogenesis of HTX.[67,68] Hence, we analyzed the length of primary cilia in *PNPLA4*-overexpressing AC16 cells. Representative images of the primary cilia of both *PNPLA4*-overexpressing and control AC16 cells are shown in Figure 6C. Using ImageJ, we measured cilia length, which showed that *PNPLA4* overexpression resulted in significantly shorter primary cilia [Figure 6C] (2.187 ± 0.727 *vs.* 1.258 ± 0.383, $t = 6.171$, $P < 0.0001$). This finding confirmed the notion that primary cilia formation was indeed compromised in *PNPLA4*-overexpressing AC16 cells.

To test whether pharmacologically lowering ATP production would rescue primary cilia defect, we treated cells with rotenone (0.2 μmol/L in DMSO), a natural inhibitor of the mitochondrial electron transport chain, to evaluate primary cilia assembly. As shown in Figure 6D, the primary cilia length was significantly improved in rotenone-treated *PNPLA4*-overexpressing AC16 cells (1.009 ± 0.327 *vs.* 2.393 ± 0.330, $t = 9.847$, $P < 0.0001$). Collectively, these data provide strong evidence that increased expression of *PNPLA4* results in aberrant ATP overproduction, which subsequently leads to the shortening of primary cilia; in this way, a higher genetic dose of *PNPLA4* can likely impact left–right patterning in the early development stage and cardiogenesis at later stages.

Discussion

HTX is one of the major birth defects associated with CHD in humans.[69] In this study, we established an HTX/CHD cohort and analyzed the potential genetic burden of rare CNVs in HTX/CHD patients. Our data revealed that 12.5% of patients in our cohort harbored CNVs, which is lower than the 23.7% previously reported for HTX/CHD[22] but higher than that for sporadic CHDs.[70] However, 7 of the 15 rare genic CNVs were known to be

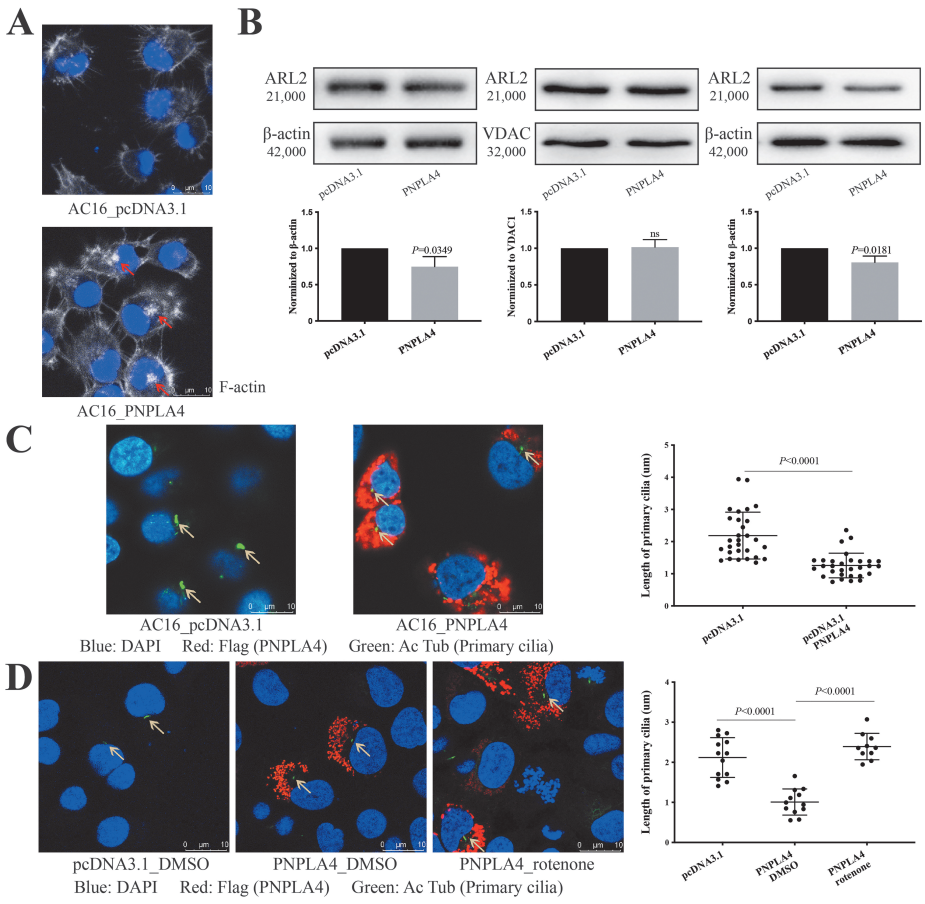

Figure 6: Altered primary cilia in *PNPLA4*-overexpressing AC16 cells. (A) ICC/IF demonstrated F-actin distribution in AC16_*PNPLA4* cells, showing elevated intracellular accumulation of F-actin patches; (B) Representative Western blot of cytoplasmic left panel; mitochondrial middle panel; and cytoplasmic excluding mitochondrial right panel. ARL2 expression. B-actin was used as a reference for cytoplasmic proteins, while VDAC was used for mitochondrial proteins; (C) Representative images of the AC16 and AC16_*PNPLA4* groups. Primary cilia were stained with an anti-acetylated tubulin antibody (green), as indicated by the arrows, and PNPLA4 was visualized with a DYKDDDDK tag antibody (red). *PNPLA4* overexpression caused a decrease in the length of the primary cilium; (D) Cilia were elongated after the repression of ATP synthesis by rotenone. An acetylated tubulin antibody was used to stain primary cilia (green, arrows), and a DYKDDDDK tag antibody was used to stain PNPLA4 (red). ATP: Adenosine triphosphate.

recurrent and associated with specific syndromes: the *de novo* 15q13.3 deletion included *CHRNA7*, which is associated with CHD,[71] and the 22q11.2 deletion included *TBX1* and *CRKL*, which contribute to DiGeorge syndrome.[72] Thus, these CNVs are likely the main genetic factors contributing to CHD phenotypes in our HTX/CHD patients. Whether these CNVs also contribute to HTX needs to be further validated. Whole-exome sequencing will be used to determine the additional genetic factors in these patients that lead to these complex HTX/CHD phenotypes. Interestingly, eight other unique genic CNVs were identified in our HTX/CHD cohort. In particular, the X-chromosome linked Xp22.31 duplication attracted our attention, partly because HTX is known to be associated with X-linked genes, such as *ZIC3*, leading to the possibility that Xp22.31 duplication is another X-linked HTX-related variant. Although the Xp22.31 duplication region has been reported to be frequently rearranged and to occur at a certain frequency in the healthy population, one study revealed that, in a specific disease population, Xp22.31 duplication occurred at a greater frequency (0.37%) in the disease group, which included intellectual disability, autism, dysmorphic features, and/or multiple congenital anomalies, than in the healthy control group (0.15%).[73] This finding appeared to be consistent with a more recent study based on data from the UK Biobank, in which male Xp22.31 duplication carriers had a higher prevalence of inguinal hernia and mania/bipolar disorder (1.9% and 1.0%, respectively).[74] Therefore, we cannot exclude the possibility that Xp22.31 duplication is a risk factor for certain diseases with complex genetic backgrounds. In addition, based on the DECIPHER database, *PNPLA4* is potentially associated with CHDs, which raises the immediate question of whether this CNV event is related to HTX, CHD, or both. This study aimed to answer this question by investigating the biological functions that are potentially altered by elevated *PNPLA4* expression.

PNPLA4 is a phospholipase that is involved in triglyceride and retinylester hydrolysis and is known for its function in mitochondria-mediated energy metabolism.[37,39] Few reports have been published regarding the association between disease and variations in *PNPLA4*. For example, SNPs in *PNPLA4* may be associated with gastrointestinal disorders in men and asthma and anemia in women.[75] Additionally, the expression of *PNPLA4* is significantly lower in patients with relapsed/refractory multiple

myeloma than in those with newly diagnosed multiple myeloma.[76] Among other members of the *PNPLA* gene family, mutations in *PNPLA2* may lead to neutral lipid storage disease with myopathy[77]; moreover, the *PNPLA3* I148M polymorphism is associated with non-alcoholic fatty liver disease.[78] Surprisingly, there is no mouse homolog of *PNPLA4*, suggesting that the function of this phospholipase is redundant among some members of this family in mice. To determine the potential role of *PNPLA4* in cardiac development, we first used a human iPSC-cardiomyocyte differentiation system and analyzed the expression pattern of *PNPLA4* during the differentiation process. As shown in Figure 2, the unique pattern of *PNPLA4* expression suggested that it is involved in both embryonic developmental process at early stage and the cardiomyocyte differentiation/maturation at a later stage; in particular, its pattern is similar to that of *ACVR2B*, a critical gene involved in left–right patterning.[43] We also examined the *PNPLA4* expression pattern in early human embryos via reanalysis of previously published scRNA-seq data (GSE157329).[32] Among the *PNPLA* family members, only *PNPLA4* was enriched in specific clusters in early human embryos, suggesting a possible role for *PNPLA4* in early embryonic development. Based on the annotation for the developmental system from the original article,[32] we identified that *PNPLA4* expression is associated with cell lineages (Clusters 3, 11, and 16) related to early left–right patterning (lateral plate mesoderm) as well as with Cluster 9 related to the neural crest, which contributes to cardiac cell lineages. Hence, these findings reinforce the notion that *PNPLA4* may contribute to the pathogenesis of CHD/HTX.

By generating *PNPLA4*-overexpressing hiPSCs, we further tested the biological impact of elevated expression levels of *PNPLA4* on hiPSC-cardiomyocyte differentiation. Our genome-wide transcriptomic analysis demonstrated that the early patterning process was affected by the overexpression of *PNPLA4*; in particular, genes critically involved in left–right asymmetrical development, including *LEF1, NOG, ZIC3, and ARMC4*, as well as genes related to cilium and microtube cytoskeletal network formation and function, were altered [Figure 3 and Supplementary Figure 2, http://links.lww.com/CM9/C59]. These findings strongly suggest that a higher genetic dose of *PNPLA4* likely alters early development, which further suggests that Xp22.31 duplication may indeed contribute to HTX and CHDs. Additional findings also suggest that altered energy metabolism and ATP production are likely causal mechanisms at the molecular level.

We further validated our findings using two additional sets of experiments. First, we used transgenic zebrafish as an *in vivo* model system to test the biological effect of increased *pnpla4* expression. The data confirmed the observation from the hiPSC experiment. Second, we used the human cardiomyocyte cell line AC16 to validate the alterations in metabolic pathways and ciliary function induced by a high dose of *PNPLA4*. Our data confirmed elevated intracellular ATP levels and demonstrated that reducing ATP levels can effectively offset altered primary cilium length. Collectively, our study provides a series of data suggesting that Xp22.31 duplication contributes to HTX/CHDs by the enhanced level of ATP production and the dysfunctional primary cilia. However, it is not yet clear how ATP elevation results in shortened cilia. Because ATP-dependent F-actin polymerization may impose a physical obstacle to ciliogenesis,[60] the observed alteration in ATPase activity and the accumulation of F-actin patches may explain this phenotype. Abnormal hydrolysis of ATP and increased ATP-bound actin available for polymerization may cause perturbed F-actin and cilia[60] and ultimately lead to HTX/CHDs.

In summary, our findings provide further insights into the association of CNVs with the development of HTX/CHD. Our *in vivo* and *in vitro* data suggest that the elevated level of *PNPLA4* expression can alter developmental patterning and cardiac development, which leads to HTX/CHDs. Altered ATP production and primary cilia formation and function are likely disease-causing mechanisms.

Acknowledgments

We would like thank Dr. Qiu Jiang for providing support on zebrafish experiments. We thank Medical Science Data Center of Fudan University for providing bioinformatics analysis support.

Funding

This work was supported by the National Key Research and Development Project of China (No.2021YFC2701000), Natural Science Foundation of China (Nos.82270312 and 82370309), Shanghai Basic Research Project of Science and Technology Innovation Action Plan (No. 20JC1418300), and CAMS Innovation Fund for Medical Sciences (No.2019-I2M-5-002).

Conflicts of interest

None.

References

1. Lin AE, Ticho BS, Houde K, Westgate MN, Holmes LB. Heterotaxy: Associated conditions and hospital-based prevalence in newborns. Genet Med 2000;2:157–172. doi: 10.1097/00125817-200005000-00002.
2. Mishra S. Cardiac and non-cardiac abnormalities in heterotaxy syndrome. Indian J Pediatr 2015;82:1135–1146. doi: 10.1007/s12098-015-1925-x.
3. Zhao QM, Liu F, Wu L, Ma XJ, Niu C, Huang GY. Prevalence of congenital heart disease at live birth in China. J Pediatr 2019;204:53–58. doi: 10.1016/j.jpeds.2018.08.040.
4. Lin AE, Krikov S, Riehle-Colarusso T, Frías JL, Belmont J, Anderka M, *et al*. Laterality defects in the national birth defects prevention study (1998-2007): Birth prevalence and descriptive epidemiology. Am J Med Genet A 2014;164A:2581–2591. doi: 10.1002/ajmg.a.36695.
5. Swisher M, Jonas R, Tian X, Lee ES, Lo CW, Leatherbury L. Increased postoperative and respiratory complications in patients with congenital heart disease associated with heterotaxy. J Thorac Cardiovasc Surg 2011;141:637–44,644.e1–3. doi: 10.1016/j.jtcvs.2010.07.082.
6. Stoll C, Dott B, Alembik Y, Roth MP. Associated noncardiac congenital anomalies among cases with congenital heart defects. Eur J Med Genet 2015;58:75–85. doi: 10.1016/j.ejmg.2014.12.002.
7. Li S, Liu S, Chen W, Yuan Y, Gu R, Song Y, *et al*. A novel ZIC3 gene mutation identified in patients with heterotaxy and congenital

heart disease. Sci Rep 2018;8:12386. doi: 10.1038/s41598-018-30204-3.
8. French VM, van de Laar IM, Wessels MW, Rohe C, Roos-Hesselink JW, Wang G, *et al*. NPHP4 variants are associated with pleiotropic heart malformations. Circ Res 2012;110:1564–1574. doi: 10.1161/circresaha.112.269795.
9. Hornef N, Olbrich H, Horvath J, Zariwala MA, Fliegauf M, Loges NT, *et al*. DNAH5 mutations are a common cause of primary ciliary dyskinesia with outer dynein arm defects. Am J Respir Crit Care Med 2006;174:120–126. doi: 10.1164/rccm.200601-084OC.
10. Kosaki K, Bassi MT, Kosaki R, Lewin M, Belmont J, Schauer G, *et al*. Characterization and mutation analysis of human LEFTY A and LEFTY B, homologues of murine genes implicated in left-right axis development. Am J Hum Genet 1999;64:712–721. doi: 10.1086/302289.
11. Mohapatra B, Casey B, Li H, Ho-Dawson T, Smith L, Fernbach SD, *et al*. Identification and functional characterization of NODAL rare variants in heterotaxy and isolated cardiovascular malformations. Hum Mol Genet 2009;18:861–871. doi: 10.1093/hmg/ddn411.
12. Negretti MI, Böse N, Petri N, Kremnyov S, Tsikolia N. Nodal asymmetry and hedgehog signaling during vertebrate left-right symmetry breaking. Front Cell Dev Biol 2022;10:957211. doi: 10.3389/fcell.2022.957211.
13. Montague TG, Gagnon JA, Schier AF. Conserved regulation of Nodal-mediated left-right patterning in zebrafish and mouse. Development 2018;145:dev171090. doi: 10.1242/dev.171090.
14. Hamada H. Roles of motile and immotile cilia in left-right symmetry breaking. In: Nakanishi T, Markwald RR, Baldwin HS, Keller BB, Srivastava D, Yamagishi H, eds. Etiology and morphogenesis of congenital heart disease: From gene function and cellular interaction to morphology. Tokyo: Springer; 2016: 57–65.
15. Mill P, Christensen ST, Pedersen LB. Primary cilia as dynamic and diverse signalling hubs in development and disease. Nat Rev Genet 2023;24:421–441. doi: 10.1038/s41576-023-00587-9.
16. Tabin CJ, Vogan KJ. A two-cilia model for vertebrate left-right axis specification. Genes Dev 2003;17:1–6. doi: 10.1101/gad.1053803.
17. Klena NT, Gibbs BC, Lo CW. Cilia and ciliopathies in congenital heart disease. Cold Spring Harb Perspect Biol 2017;9:a028266. doi: 10.1101/cshperspect.a028266.
18. Pierpont ME, Brueckner M, Chung WK, Garg V, Lacro RV, McGuire AL, *et al*. Genetic basis for congenital heart disease: Revisited: A scientific statement from the American Heart Association. Circulation 2018;138:e653–e711. doi: 10.1161/cir.0000000000000606.
19. Savory K, Manivannan S, Zaben M, Uzun O, Syed YA. Impact of copy number variation on human neurocognitive deficits and congenital heart defects: A systematic review. Neurosci Biobehav Rev 2020;108:83–93. doi: 10.1016/j.neubiorev.2019.10.020.
20. Verbitsky M, Westland R, Perez A, Kiryluk K, Liu Q, Krithivasan P, *et al*. The copy number variation landscape of congenital anomalies of the kidney and urinary tract. Nat Genet 2019;51:117–127. doi: 10.1038/s41588-018-0281-y.
21. Costain G, Silversides CK, Bassett AS. The importance of copy number variation in congenital heart disease. NPJ Genom Med 2016;1:16031. doi: 10.1038/npjgenmed.2016.31.
22. Liu C, Cao R, Xu Y, Li T, Li F, Chen S, *et al*. Rare copy number variants analysis identifies novel candidate genes in heterotaxy syndrome patients with congenital heart defects. Genome Med 2018;10:40. doi: 10.1186/s13073-018-0549-y.
23. Cowan JR, Tariq M, Shaw C, Rao M, Belmont JW, Lalani SR, *et al*. Copy number variation as a genetic basis for heterotaxy and heterotaxy-spectrum congenital heart defects. Philos Trans R Soc Lond B Biol Sci 2016;371:20150406. doi: 10.1098/rstb.2015.0406.
24. Cervantes-Salazar J, Curi-Curi P, Ramírez-Marroquín S, Calderón-Colmenero J, Munoz-Castellanos L. Anatomic diagnosis of congenital heart disease. A practical approach based on the sequentiality principle. Arch Cardiol Mex 2010;80:119–125.
25. Molck MC, Simioni M, Paiva Vieira T, Sgardioli IC, Paoli Monteiro F, Souza J, *et al*. Genomic imbalances in syndromic congenital heart disease. J Pediatr (Rio J) 2017;93:497–507. doi: 10.1016/j.jped.2016.11.007.
26. Wang Q, Yang H, Bai A, Jiang W, Li X, Wang X, *et al*. Functional engineered human cardiac patches prepared from nature's platform improve heart function after acute myocardial infarction. Biomaterials 2016;105:52–65. doi: 10.1016/j.biomaterials.2016.07.035.
27. Zhan Y, Sun X, Li B, Cai H, Xu C, Liang Q, *et al*. Establishment of a PRKAG2 cardiac syndrome disease model and mechanism study using human induced pluripotent stem cells. J Mol Cell Cardiol 2018;117:49–61. doi: 10.1016/j.yjmcc.2018.02.007.
28. Zhang M, Zhang J, Lin SC, Meng A. β-Catenin 1 and β-catenin 2 play similar and distinct roles in left-right asymmetric development of zebrafish embryos. Development 2012;139:2009–2019. doi: 10.1242/dev.074435.
29. Amack JD, Yost HJ. The T box transcription factor no tail in ciliated cells controls zebrafish left-right asymmetry. Curr Biol 2004;14:685–690. doi: 10.1016/j.cub.2004.04.002.
30. Bhattacharya S, Burridge PW, Kropp EM, Chuppa SL, Kwok WM, Wu JC, *et al*. High efficiency differentiation of human pluripotent stem cells to cardiomyocytes and characterization by flow cytometry. J Vis Exp 2014;91:52010. doi: 10.3791/52010.
31. Xia J, Wishart DS. MetPA: A web-based metabolomics tool for pathway analysis and visualization. Bioinformatics 2010;26:2342–2344. doi: 10.1093/bioinformatics/btq418.
32. Xu Y, Zhang T, Zhou Q, Hu M, Qi Y, Xue Y, *et al*. A single-cell transcriptome atlas profiles early organogenesis in human embryos. Nat Cell Biol 2023;25:604–615. doi: 10.1038/s41556-023-01108-w.
33. Viuff M, Skakkebæk A, Johannsen EB, Chang S, Pedersen SB, Lauritsen KM, *et al*. X chromosome dosage and the genetic impact across human tissues. Genome Med 2023;15:21. doi: 10.1186/s13073-023-01169-4.
34. Reed MJ, Purohit A, Woo LW, Newman SP, Potter BV. Steroid sulfatase: Molecular biology, regulation, and inhibition. Endocr Rev 2005;26:171–202. doi: 10.1210/er.2004-0003.
35. Lahn BT, Page DC. A human sex-chromosomal gene family expressed in male germ cells and encoding variably charged proteins. Hum Mol Genet 2000;9:311–319. doi: 10.1093/hmg/9.2.311.
36. Holmes RS. Vertebrate patatin-like phospholipase domain-containing protein 4 (PNPLA4) genes and proteins: A gene with a role in retinol metabolism. 3 Biotech 2012;2:277–286. doi: 10.1007/s13205-012-0063-7.
37. Kohda M, Tokuzawa Y, Kishita Y, Nyuzuki H, Moriyama Y, Mizuno Y, *et al*. A comprehensive genomic analysis reveals the genetic landscape of mitochondrial respiratory chain complex deficiencies. PLoS Genet 2016;12:e1005679. doi: 10.1371/journal.pgen.1005679.
38. Kienesberger PC, Oberer M, Lass A, Zechner R. Mammalian patatin domain containing proteins: A family with diverse lipolytic activities involved in multiple biological functions. J Lipid Res 2009;50(Suppl):S63–8. doi: 10.1194/jlr.R800082-JLR200.
39. Gao JG, Shih A, Gruber R, Schmuth M, Simon M. GS2 as a retinol transacylase and as a catalytic dyad independent regulator of retinylester accretion. Mol Genet Metab 2009;96:253–260. doi: 10.1016/j.ymgme.2008.12.007.
40. Gao JG, Simon M. A comparative study of human GS2, its paralogues, and its rat orthologue. Biochem Biophys Res Commun 2007;360:501–506. doi: 10.1016/j.bbrc.2007.06.089.
41. Kumar L, Futschik ME. Mfuzz: A software package for soft clustering of microarray data. Bioinformation 2007;2:5–7. doi: 10.6026/97320630002005.
42. Hjeij R, Lindstrand A, Francis R, Zariwala MA, Liu X, Li Y, *et al*. ARMC4 mutations cause primary ciliary dyskinesia with randomization of left/right body asymmetry. Am J Hum Genet 2013;93:357–367. doi: 10.1016/j.ajhg.2013.06.009.
43. Ma L, Selamet Tierney ES, Lee T, Lanzano P, Chung WK. Mutations in ZIC3 and ACVR2B are a common cause of heterotaxy and associated cardiovascular anomalies. Cardiol Young 2012;22:194–201. doi: 10.1017/s1047951111001181.
44. Tsiairis CD, McMahon AP. An Hh-dependent pathway in lateral plate mesoderm enables the generation of left/right asymmetry. Curr Biol 2009;19:1912–1917. doi: 10.1016/j.cub.2009.09.057.
45. Mick DU, Rodrigues RB, Leib RD, Adams CM, Chien AS, Gygi SP, *et al*. Proteomics of primary cilia by proximity labeling. Dev Cell 2015;35:497–512. doi: 10.1016/j.devcel.2015.10.015.
46. Zhu P, Xu X, Lin X. Both ciliary and non-ciliary functions of Foxj1a confer Wnt/β-catenin signaling in zebrafish left-right patterning. Biol Open 2015;4:1376–1386. doi: 10.1242/bio.012088.
47. Mine N, Anderson RM, Klingensmith J. BMP antagonism is required in both the node and lateral plate mesoderm for mammalian left-right axis establishment. Development 2008;135:2425–2434. doi: 10.1242/dev.018986.
48. Heller S, Penrose HM, Cable C, Biswas D, Nakhoul H, Baddoo M, *et al*. Reduced mitochondrial activity in colonocytes facilitates AMPKα2-dependent inflammation. FASEB J 2017;31:2013–2025. doi: 10.1096/fj.201600976R.

49. Salminen A, Kaarniranta K, Kauppinen A. Regulation of longevity by FGF21: Interaction between energy metabolism and stress responses. Ageing Res Rev 2017;37:79–93. doi: 10.1016/j.arr.2017.05.004.
50. Haemmerle G, Moustafa T, Woelkart G, Büttner S, Schmidt A, van de Weijer T, *et al*. ATGL-mediated fat catabolism regulates cardiac mitochondrial function via PPAR-α and PGC-1. Nat Med 2011;17:1076–1085. doi: 10.1038/nm.2439.
51. Anderson G, Mazzoccoli G. Left ventricular hypertrophy: Roles of mitochondria CYP1B1 and melatonergic pathways in co-ordinating wider pathophysiology. Int J Mol Sci 2019;20:4068. doi: 10.3390/ijms20164068.
52. Matsui T, Ishikawa H, Bessho Y. Cell collectivity regulation within migrating cell cluster during Kupffer's vesicle formation in zebrafish. Front Cell Dev Biol 2015;3:27. doi: 10.3389/fcell.2015.00027.
53. Palomer X, Román-Azcona MS, Pizarro-Delgado J, Planavila A, Villarroya F, Valenzuela-Alcaraz B, *et al*. SIRT3-mediated inhibition of FOS through histone H3 deacetylation prevents cardiac fibrosis and inflammation. Signal Transduct Target Ther 2020;5:14. doi: 10.1038/s41392-020-0114-1.
54. Huang Z, Xie N, Illes P, Di Virgilio F, Ulrich H, Semyanov A, *et al*. From purines to purinergic signalling: Molecular functions and human diseases. Signal Transduct Target Ther 2021;6:162. doi: 10.1038/s41392-021-00553-z.
55. Wang D, Wang F, Shi KH, Tao H, Li Y, Zhao R, *et al*. Lower circulating folate induced by a fidgetin intronic variant is associated with reduced congenital heart disease susceptibility. Circulation 2017;135:1733–1748. doi: 10.1161/circulationaha.116.025164.
56. Fassett JT, Xu X, Kwak D, Wang H, Liu X, Hu X, *et al*. Microtubule actin cross-linking factor 1 regulates cardiomyocyte microtubule distribution and adaptation to hemodynamic overload. PLoS One 2013;8:e73887. doi: 10.1371/journal.pone.0073887.
57. Moudgil R, Samra G, Ko KA, Vu HT, Thomas TN, Luo W, *et al*. Topoisomerase 2B decrease results in diastolic dysfunction via p53 and Akt: A novel pathway. Front Cardiovasc Med 2020;7:594123. doi: 10.3389/fcvm.2020.594123.
58. Tigchelaar W, de Jong AM, Bloks VW, van Gilst WH, de Boer RA, Silljé HH. Hypertrophy induced KIF5B controls mitochondrial localization and function in neonatal rat cardiomyocytes. J Mol Cell Cardiol 2016;97:70–81. doi: 10.1016/j.yjmcc.2016.04.005.
59. Piquereau J, Novotova M, Fortin D, Garnier A, Ventura-Clapier R, Veksler V, *et al*. Postnatal development of mouse heart: Formation of energetic microdomains. J Physiol 2010;588:2443–2454. doi: 10.1113/jphysiol.2010.189670.
60. Smith CEL, Lake AVR, Johnson CA. Primary cilia, ciliogenesis and the actin cytoskeleton: A little less resorption, a little more actin please. Front Cell Dev Biol 2020;8:622822. doi: 10.3389/fcell.2020.622822.
61. Oosterheert W, Klink BU, Belyy A, Pospich S, Raunser S. Structural basis of actin filament assembly and aging. Nature 2022;611:374–379. doi: 10.1038/s41586-022-05241-8.
62. Pollard TD. Actin and actin-binding proteins. Cold Spring Harb Perspect Biol 2016;8:a018226. doi: 10.1101/cshperspect.a018226.
63. Streets AJ, Prosseda PP, Ong AC. Polycystin-1 regulates ARHGAP35-dependent centrosomal RhoA activation and ROCK signaling. JCI Insight 2020;5:e135385. doi: 10.1172/jci.insight.135385.
64. Lechtreck KF. IFT-cargo interactions and protein transport in cilia. Trends Biochem Sci 2015;40:765–778. doi: 10.1016/j.tibs.2015.09.003.
65. Jaiswal M, Fansa EK, Kösling SK, Mejuch T, Waldmann H, Wittinghofer A. Novel biochemical and structural insights into the interaction of myristoylated cargo with Unc119 protein and their release by Arl2/3. J Biol Chem 2016;291:20766–20778. doi: 10.1074/jbc.M116.741827.
66. Meyer JN, Leuthner TC, Luz AL. Mitochondrial fusion, fission, and mitochondrial toxicity. Toxicology 2017;391:42–53. doi: 10.1016/j.tox.2017.07.019.
67. Burkhalter MD, Sridhar A, Sampaio P, Jacinto R, Burczyk MS, Donow C, *et al*. Imbalanced mitochondrial function provokes heterotaxy via aberrant ciliogenesis. J Clin Invest 2019;129:2841–2855. doi: 10.1172/jci98890.
68. Supp DM, Brueckner M, Kuehn MR, Witte DP, Lowe LA, McGrath J, *et al*. Targeted deletion of the ATP binding domain of left-right dynein confirms its role in specifying development of left-right asymmetries. Development 1999;126:5495–5504. doi: 10.1242/dev.126.23.5495.
69. Sempou E, Khokha MK. Genes and mechanisms of heterotaxy: Patients drive the search. Curr Opin Genet Dev 2019;56:34–40. doi: 10.1016/j.gde.2019.05.003.
70. Soemedi R, Wilson IJ, Bentham J, Darlay R, Töpf A, Zelenika D, *et al*. Contribution of global rare copy-number variants to the risk of sporadic congenital heart disease. Am J Hum Genet 2012;91:489–501. doi: 10.1016/j.ajhg.2012.08.003.
71. Lowther C, Costain G, Stavropoulos DJ, Melvin R, Silversides CK, Andrade DM, *et al*. Delineating the 15q13.3 microdeletion phenotype: A case series and comprehensive review of the literature. Genet Med 2015;17:149–157. doi: 10.1038/gim.2014.83.
72. Sullivan KE. Chromosome 22q11.2 deletion syndrome and DiGeorge syndrome. Immunol Rev 2019;287:186–201. doi: 10.1111/imr.12701.
73. Li F, Shen Y, Köhler U, Sharkey FH, Menon D, Coulleaux L, *et al*. Interstitial microduplication of Xp22.31: Causative of intellectual disability or benign copy number variant? Eur J Med Genet 2010;53:93–99. doi: 10.1016/j.ejmg.2010.01.004.
74. Gubb SJA, Brcic L, Underwood JFG, Kendall KM, Caseras X, Kirov G, *et al*. Medical and neurobehavioural phenotypes in male and female carriers of Xp22.31 duplications in the UK Biobank. Hum Mol Genet 2020;29:2872–2881. doi: 10.1093/hmg/ddaa174.
75. Wren G, Baker E, Underwood J, Humby T, Thompson A, Kirov G, *et al*. Characterising heart rhythm abnormalities associated with Xp22.31 deletion. J Med Genet 2023;60:636–643. doi: 10.1136/jmg-2022-108862.
76. Kumari R, Majumder MM, Lievonen J, Silvennoinen R, Anttila P, Nupponen NN, *et al*. Prognostic significance of esterase gene expression in multiple myeloma. Br J Cancer 2021;124:1428–1436. doi: 10.1038/s41416-020-01237-1.
77. Fischer J, Lefèvre C, Morava E, Mussini JM, Laforêt P, Negre-Salvayre A, *et al*. The gene encoding adipose triglyceride lipase (PNPLA2) is mutated in neutral lipid storage disease with myopathy. Nat Genet 2007;39:28–30. doi: 10.1038/ng1951.
78. Basu Ray S. PNPLA3-I148M: A problem of plenty in non-alcoholic fatty liver disease. Adipocyte 2019;8:201–208. doi: 10.1080/21623945.2019.1607423.

How to cite this article: Gao H, Huang XH, Chen WC, Feng ZY, Zhao ZS, Li P, Tan CZ, Wang JX, Zhuang QN, Gao Y, Min SJ, Yao QY, Qian MX, Ma XJ, Wu FZ, Yan WL, Sheng W, Huang GY. Association of copy number variation in X chromosome-linked *PNPLA4* with heterotaxy and congenital heart disease. Chin Med J 2024;137:1823–1834. doi: 10.1097/CM9.0000000000003192